Vol. 84: 1–21, 2021
https://doi.org/10.3354/cr01651

CLIMATE RESEARCH
Clim Res

Published online June 3

Ocean–Land Atmosphere Model (OLAM) performance for major extreme meteorological events near the coastal region of southern Brazil

D. C. de Souza[1,2,*], R. Ramos da Silva[1]

[1]Climate and Meteorology Laboratory, Department of Physics, Federal University of Santa Catarina, Florianópolis, SC 88040-900, Brazil

[2]*Present address:* Astronomy, Geophysics and Atmospheric Sciences Institute, São Paulo University, São Paulo, SP 05508-090, Brazil

ABSTRACT: Coastal regions are generally densely populated and have become highly vulnerable to the occurrence of extreme events. In recent years, Brazil's southern coastal region has been affected by several different extreme weather events that have caused coastal flooding, with economic losses as well as fatalities. Understanding and improving the predictability of these events has become a major issue for the local population. In this study, state-of-the-art numerical modeling was applied to this region to assess the ability of the Ocean–Land Atmosphere Model to represent major extreme events. The model was applied to the region with a high-resolution grid refinement technique capable of simultaneously representing global and local atmospheric phenomena. The main events that affected Brazil's southern coastal region between 2000 and 2018 were identified and then simulated. All selected events were associated with cyclonic and/or anticyclonic systems near the coastal region of the study area. Those systems were responsible for bringing heavy rain, strong winds and sea level rise, causing impacts for the coastal region. The results of the numerical simulations were compared with observational data to evaluate model performance. The model simulated well the air temperature and wind fields. Correlation values for sea level pressure were high despite a maximum positive bias of approximately 2 hPa. Precipitation presented a negative bias for most events. Finally, the results show that the methodology allowed for a detailed representation of sensible and latent heat fluxes for the region, allowing a better representation of local mesoscale features.

KEY WORDS: Numerical modeling · Cyclone · Anticyclone · Extreme precipitation · Extreme winds · Model validation · Coastal flooding · Hurricane Catarina

1. INTRODUCTION

In the near future, a global increase is expected in the frequency and intensity of extreme weather and climate events (IPCC 2013). This poses a concerning scenario for our society, as extreme events can be a source of risk for populations. For instance, between 1998 and 2017, climate-related hazards accounted for more than US$2 trillion of losses worldwide, affecting more than 4 billion people (Wallemacq & House 2018). Societal changes during the previous century such as the rapid increase of human population in coastal and low-lying areas have made communities more exposed and vulnerable to the impacts of such extreme events (Karl & Easterling 1999, Kunkel et al. 1999, Easterling et al. 2000, Mechler & Bouwer 2015). In developing countries, extreme events are a great source of fatalities and economic losses, as the population and governments are less resilient, adapted and prepared (Handmer et al. 2012).

*Corresponding author: danilo.oceano@gmail.com

The southern region of Brazil (SBr), composed of the states of Paraná (PR), Santa Catarina (SC) and Rio Grande do Sul (RS), is a region which suffered very high economic losses due to the meteorological extreme events of recent years (World Bank 2016). The coastal region of those states is inhabited by about 3.2 million people, and the area has developed important economic and technological activities (Strohaecker 2004) as well as 21% of all Brazilian seaports. The impacts of extreme events in this area can be devastating, as urbanized coastal low-lying areas are vulnerable to events such as extreme precipitation and storm surges. Examples of such events were Hurricane Catarina in 2004 and the Itajaí Valley (northeast of SC) flooding in 2008. Both events directly affected millions of people due to inundations, landslides and high wind speeds that caused property loss, heavy damage to local infrastructure and fatalities (Nunes & da Silva 2013, Hermann 2014, World Bank 2016).

The weather in this region is related to phenomena of large regional and local scales. Such phenomena include Rossby wave propagation (which affect the propagation of mid-latitude cold fronts), the South Atlantic Anticyclone (SAAC) (Garreaud et al. 2009), extratropical cyclones (ECs) (Reboita et al. 2018), cold fronts (Compagnucci & Salles 1997, Garreaud 2000, Garreaud et al. 2009), the South Atlantic Convergence Zone (Kodama 1992, Carvalho et al. 2004, Garreaud et al. 2009, Fernandes & Rodrigues 2018), the South American Low-Level Jet east of the Andes (Seluchi & Marengo 2000, Salio 2002, Seluchi et al. 2003, Marengo et al. 2004, Salio et al. 2007), the Brazil-Malvinas Confluence (Gordon 1989, Stramma 1989, Gramcianinov et al. 2019), local orographic effects (Rodrigues & Ynoue 2016), heterogeneities in topography and land use (as seen in Fig. 1D) and land–sea breeze circulations. Therefore, models aiming to reproduce the occurrence of extreme events in this region should be able to represent multiple scales and the interaction between them.

The western South Atlantic Ocean (SAO) is very cyclogenetic, and there are 3 preferable regions for EC genesis (Fig. 1A): south-southeastern Brazil (RG1), extreme south Brazil and Uruguay (RG2) and southeast Argentina (RG3) near 45° S (Sinclair 1995, Hoskins & Hodges 2005, Mendes et al. 2010, Reboita et al. 2012, Gramcianinov et al. 2019). Between 20 and 30% of annual precipitation in the SBr region is due to ECs occurring in the vicinity of this area (Reboita et al. 2018). Also, ECs are responsible for the occurrence of intense winds, high sea waves (extreme sea waves, in some cases) and storm surges along the Brazilian coast, triggering episodes of coastal flooding and beach erosion (Parise et al. 2009, Campos et al. 2010, Machado et al. 2010, Parise & Farina 2012, Guimarães et al. 2014, Gomes da Silva et al. 2016, Albuquerque et al. 2018).

Climate projections indicate heterogeneous changes in EC occurrence over the SAO area. Mean cyclogenesis in the SAO might become less active, especially for the most intense systems (Krüger et al. 2012, Reboita et al. 2018). This might be related to a poleward shift of the upper polar jet (Reboita et al. 2018) and the enhancement of winds related to the SAAC (Krüger et al. 2012). However, for the 2 cyclogenetic foci located closest to the Brazilian coast (RG1 and RG2), climate projections indicate a possible increase in cyclogenesis (Reboita et al. 2018). Nevertheless, climate model projections suggest an overall increase in temperature and precipitation for coastal SBr, with wetter summers and drier winters (Krüger et al. 2012, Chou et al. 2014, Ramos da Silva & Haas

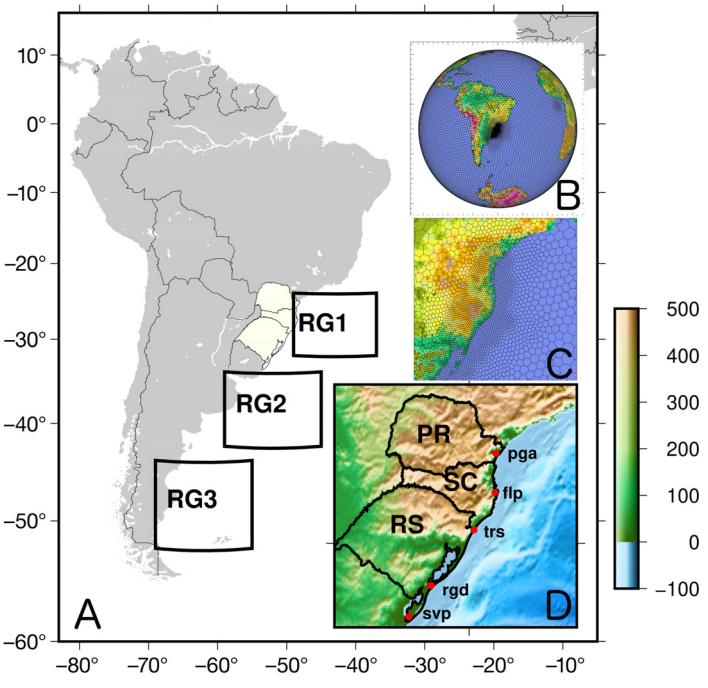

Fig. 1. (A) South America, the southern Brazil study area (highlighted) and the 3 cyclogenetic regions (RG) in the western South Atlantic (see Section 1 for details). (B) Global computational grid used for Ocean–Land Atmosphere Model numerical experiments. (C) High-resolution regional grid centered on the coastal region of southern Brazil. (D) Southern Brazil topography (m); borders of Paraná (PR), Santa Catarina (SC) and Rio Grande do Sul (RS) states; and Brazilian National Institute for Space Research Center of Weather Forecast and Climate Studies (INPE) meteorological stations used for model validation (red dots). Cities where the stations are located: pga: Paranaguá; flp: Florianópolis; trs: Torres; rgd: Rio Grande; svp: Santa Vitoria do Palmar

2016), and more frequent and intense extreme precipitation events, increasing the risk of floods in the region (Marengo et al. 2009, Nuñez et al. 2009, Chou et al. 2014).

As extreme events in the SBr, such as Hurricane Catarina and the Itajaí Valley flooding in 2008, had caused very high economic and societal costs (Nunes & da Silva 2013, Hermann 2014, World Bank 2016), responsible authorities need a local assessment of the possible future occurrence of similar extreme events. The main tools used in long-term climatic studies are general circulation models (GCMs), which have coarser resolutions from 50 to 450 km, that do not fully resolve the land use, land–sea distribution and complex topography of South America (Taylor et al. 2012). Also, this level of resolution is not enough to explicitly simulate mesoscale processes and the smaller ECs (Reboita et al. 2018) and do not simulate well extreme precipitation events (Farnham et al. 2018). To achieve more refined spatial resolutions, 2 techniques can be used: dynamical downscaling, a process that comprehends nesting a regional climate model (RCM) into a GCM, or the statistical downscaling of GCM output.

The major studies using RCMs that have been made to estimate the future occurrence of extreme events in South America adopted a grid space from 40 to 50 km (Ambrizzi et al. 2019 and references therein) which do not fully resolve the effects of the complex topography of South America and the details of the SBr surface heterogeneity and coastline (Fig. 1D). Also, this methodology applies 1-way communication between the GCM and the RCM; thus, the local-scale phenomena do not interact with the large-scale circulation. Therefore, novel studies attempting to address future projections of extreme events for the coastal region of southern Brazil would benefit from increased horizontal model resolution and scale interaction.

An important feature of the Ocean–Land Atmosphere Model (OLAM) (Walko & Avissar 2008a,b) is its ability to simulate both local-scale weather as well as global-scale phenomena simultaneously (Fig. 1B). This is achieved by its refining grids method. The model uses a global icosahedric grid as well as high-resolution grids and therefore allows 2-way communication between the different large-scale and mesoscale processes. The refining grid methodology is useful for saving computational power when large scale needs to be represented, while still achieving fine resolutions on regions of interest (Walko & Avissar 2011, Medvigy et al. 2013). Also, a better representation of South American topography by this methodology allows a more realistic representation of the South American climate under ENSO conditions (Medvigy et al. 2008).

The goal of the current study was first to identify the major extreme events that occurred in the coastal region of southern Brazil in recent years and then to test whether OLAM was capable of a realistic downscaling of the meteorological conditions associated with those events. This is the first study to identify and use a high-resolution regional grid to study the major extreme meteorological events in this area. The model uses input data from a coarser resolution reanalysis as initial and boundary conditions. The proposed methodology allows the representation of different scale phenomena, from large-scale features to local-scale circulations. Initially, 12 extreme regional events that occurred since the beginning of the current century were selected. After that, the simulated results were compared with observed meteorological and reanalysis data to answer the question, 'How well can OLAM downscale extreme events in the coastal region of southern Brazil when comparing to reanalysis?' The meteorological conditions related to each event can be found in Text S1 in the Supplement at www.int-res.com/articles/suppl/c084p001_supp.pdf.

2. MATERIALS AND METHODS

2.1. Numerical model description

For numerical simulations with the extreme events that impacted the SBr region, we used OLAM. This model has already been used to estimate the effects of global ocean warming on the South American climate (Ramos da Silva & Haas 2016) and the effects of Amazon deforestation on climate extremes in South America (Medvigy et al. 2012) and for weather forecasting and regional climate estimates for the Amazon region (Ramos da Silva et al. 2014a,b). Overall, the model provides a good representation of major coastal convective systems (Ramos da Silva et al. 2014a). Remarkably, a study from Khanna et al. (2017) demonstrated the effects of Amazon deforestation on regional atmospheric circulation, highlighting the utility of OLAM's variable resolution capability for studies of local-scale phenomena.

OLAM was developed at Duke University as an evolution of the Regional Atmospheric Modeling System (RAMS), so its physical parameterizations and computing structure were designed on the latter (Walko & Avissar 2008a,b). The RAMS model enables the achievement of high-resolution atmospheric simulations by the use of a nesting grids tech-

nique, making it very versatile (Pielke et al. 1992). However, in the RAMS model, the spatial scale of a simulation is limited to regional domains. Capable of performing global simulations with high-resolution regional grids, OLAM opens up new possibilities for numerical studies.

The model solves full non-hydrostatic compressible Navier-Stokes equations using the finite volume method. The grid elements are non-structured hexagons that can be further divided to increase horizontal resolution. This makes OLAM suited for mesoscale studies, as it can represent the interactions between large-scale phenomena and mesoscale processes simultaneously without adding errors from lateral boundary conditions (Walko & Avissar 2008a,b).

The model calculates turbulent fluxes related to soil and vegetation cover through the use of a submodel, the Land Ecosystem–Atmosphere Feedback (LEAF-3) model (Walko et al. 2000). As OLAM is an atmospheric model only, the model needs assimilation of SST data as an ocean forcing component.

2.2. Extreme events case selection

Due to the relativeness of the word 'extreme', the definition of what is an extreme event can often be vague and confusing. Thus, the widespread definition of an event extreme derives from climate statistics. In this case, an extreme event can be identified as some variable exceedance of a certain threshold, for example, an amount of rain above the 90th percentile of historical rainfall (Frich et al. 2002). However, sometimes the occurrence of an event, classified as extreme by this definition, might not really represent a damaging or severe event for society. For example, a hydroclimate event of persistent or heavy rain might not cause flooding due to the previous river level being low; thus, it might not necessarily cause significant impacts. As our goal was to simulate the main events for the study area based on the impacts felt by society, a distinct approach had to be considered.

We selected cases of extreme events for the coastal region of southern Brazil through the review of online news portals. This research returned a great number of damaging events that occurred in the study area, and we selected only the major events of the 21st century. We considered as a major event the cases that (1) were associated with any economic loss (as reported by the media) for the affected communities, (2) impacted at least a region in the study area (i.e. at least more than 1 city near the coast) and (3) were reported more than once by local news. Furthermore, we also performed a similar research of extreme events in the scientific literature. This was not our primary source for the chosen case study because not all extreme events that occur are indeed studied by the scientific community.

In this study, we defined the start and end days of an event based on the reports, for example, reported days of consecutive rain or occurrence of high sea waves in one place located in the study region. The approximated peak time of a given event was identified using distinct criteria. First, if the event was already described in the literature, we used the reported peak time. For the remaining cases, we first identified what kinds of impacts were associated with the event (for example, heavy precipitation) and then analyzed the corresponding meteorological data for the moment of maximum intensity of rain and/or moment of maximum wind speed. We also analyzed near-surface circulation from the NCEP Reanalysis 2 (Saha et al. 2014) and the Climatic Analysis Monitoring Bulletin (CLIMANÁLISE) from the Brazilian National Institute for Space Research Center of Weather Forecast and Climate Studies (INPE-CPTEC) so we could check the dynamical atmospheric phenomena leading to the respective extreme event. The CLIMANÁLISE bulletin can be found at http://climanalise.cptec.inpe.br/~rclimanl/boletim/. This bulletin ranges from 1994 to 2014, so for the analysis of events that occurred later than 2014, we used the INPE-CPTEC technical bulletin, available at http://tempo.cptec.inpe.br/boletimtecnico/pt.

2.3. Numerical experiment design

To simulate the selected events, we set OLAM with a global grid (Fig. 1B) with high resolution in the study area of coastal region of SBr (Fig. 1C). There were 5 levels of refining for the regional grid, apart from the global. This approach allowed the model to represent the major features of this coastal region. The spatial grid size varied from approximately 200 km for the global grid, increasing from 100 km through 50, 25, 12 and finally 6 km. This level of refinement allows representing the mesoscale features in this ocean–land interface. In the vertical, the model was set with 49 atmospheric levels, with resolutions ranging from 60 m in the lower level up to 2000 m in the upper stratospheric levels that reached 35 km high. For the soil, 21 levels were used, with spacing varying from 0.05 m near the surface up to 0.5 m, at 5 m depth. To maintain numerical stability,

we adopted a 10 s time step, which is applied for the whole domain.

The initial atmospheric conditions used to force the model were the wind fields, geopotential height, air temperature and relative air humidity, from the NCEP Climate Forecast System Reanalysis (CFSR). Those variables were updated during the simulations every 6 h into the model for a light nudging only on the model's coarser grid. No further data assimilation was performed.

For each event, we set up the simulations to start 3 d prior to the day of peak time for model adjustment. Also, the experiments were set to finish 6 d after the peak. Therefore, the experiments had a time length of 10 d in total, except for event (E) 07 and E12. During E07 (Itajaí Valley flooding in 2008), we included an extra day before the event start because there was also high precipitation on the previous day to the peak. For E12 (Hurricane Catarina), we considered peak time as the landfall moment. In this case, we started the simulations 10 d prior to this to capture the whole life cycle of this system, from cyclone genesis to landfall. This was important to better represent the atmospheric dynamics associated with this process in the study area during the early stages of cyclogenesis.

The physical parameterizations adopted included the cumulus convection parameterization (Grell & Freitas 2014), the diffusion coefficient for atmospheric fluxes parameterization (Smagorinsky 1963), the cloud microphysics parameterization (Walko et al. 1995, Meyers et al. 1997) and the short- and longwave radiation parameterization (Mlawer et al. 1997). Global data of topography, vegetation types and soil texture are used as surface boundary conditions for the respective soil–vegetation sub-models (LEAF-3).

2.4. Data

As previous mentioned, for model initialization and nudging, we used wind, temperature and humidity data from the CFSR reanalysis model. The CFSR is a global 6 h reanalysis product, ranging from 1979 to present days, with approximately 38 km of global atmospheric resolution. It also provides full coupling between the atmosphere and oceans, a sea ice model and assimilation of satellite radiance data (Saha et al. 2010, 2014). An assessment of CFSR performance can be found in Ebisuzaki & Zhang (2011) and Wang et al. (2011).

The oceanic boundary condition used was the Optimum Interpolation Sea Surface Temperature (OISST) from NOAA. The NOAA OISST is a weekly 1/4° resolution analysis product ranging from 1981 to the present that combines distinct observation sources such as buoys, ships and satellites and then applies an adjustment to remove sensor bias and compensate for differences in platform measurements (Reynolds et al. 2002, 2007). The weekly data are constructed from satellite images that are limited due to cloud obstructions, but the weekly superposition is able to cover the total global surface (Reynolds & Smith 1994).

For model performance assessment at the local level, we compared the simulated atmospheric variables with observational data from available meteorological stations for the study area (Fig. 1D). The data came from the National Institute of Meteorology (Instituto Nacional de Meteorologia [INMET]). The INMET stations used for analysis were located at Paranaguá, PR (25.53° S, 48.51° W); Florianópolis, SC (27.58° S, 48.56° W); Torres, RS (29.35° S, 49.73° W); Rio Grande, RS (32.03° S, 52.11° W); and Santa Vitória do Palmar, RS (33.51° S, 53.35° W). These stations were chosen because they presented the most homogeneous data available in the region affected by the selected events.

Another model evaluation assessment was performed using atmospheric fields capable of covering both land and oceans. For this evaluation, we compared the model data with precipitation fields from the Tropical Rainfall Measuring Mission (TRMM) and the Global Precipitation Measurement (GPM) mission and with temperature fields from the Modern-Era Retrospective Analysis for Research and Applications, Version 2 (MERRA-2). The TRMM precipitation product integrates data from 5 distinct satellite sensors to provide gridded data ranging from 50° N to 50° S in a 0.25° grid, with instantaneous values every 3 h (Huffman et al. 2007). The TRMM mission ranged from 1997 to 2015, and then it was replaced by the GPM mission. The GPM data use the IMERG algorithm, which aggregates multi-satellite data to provide 0.1° global half-hourly precipitation fields (Hou et al. 2014). In those cases, we used the 3B42RTv7 and the 3IMERGHHv06 TRMM and GPM products, respectively. The MERRA-2 reanalysis product includes the assimilation of observational data from a wide variety of sources such as gauge stations and satellite data, so the temperature fields are provided every 3 h in a 0.5° × 0.625° grid (Gelaro et al. 2017). A better description of those products can be found in other studies (Gebremichael & Krajewski 2004, Huffman et al. 2007, Liu 2016, Buchard et al. 2017, Randles et al. 2017, Wang et al. 2017, Draper et al. 2018).

2.5 Statistical analysis

To evaluate model performance on simulating the extreme events selected here, we performed a set of statistical analyses. For each event, we calculated model bias, RMSE, mean square error (MSE) and the spatial correlation index (CI). For such analysis, first, it is necessary to calculate the errors (model results minus observation, d_i) point to point, as:

$$d_i = \sum_{i=1}^{N} (P_{is} - P_{io}) \quad (1)$$

where P_{is} and P_{io} are, respectively, the model-simulated and the observed variables. Since the study area covers oceanic surfaces, reanalysis data were assumed as observations to compare with the model simulation results. To perform the statistical analysis, both data being compared are required to be in the same dimensions. Therefore, we performed a bilinear interpolation in the OLAM data, as it is the dataset containing the most grid points (i.e. the highest spatial resolution). For comparison, considering the spatial domain used here for the analysis, from 54° to 45° W and from 34° to 26° S, OLAM has 36 381 grid points, while GPM, TRMM and MERRA-2 have 7200, 1221 and 255 grid points, respectively. So, for each case being analyzed, we interpolated the OLAM data to have the same resolution as the respective reanalysis comparison.

Additionally, the MSE can be partitioned into a dissipative (MSE_{diss}) and a dispersive (MSE_{disp}) component (Takacs 1985), where the former explains amplitude errors and the latter, phase errors:

$$MSE_{tot} = MSE_{diss} + MSE_{disp} \quad (2)$$

The dissipative component in Eq. (2) can be estimated as:

$$MSE_{diss} = [\sigma(P_{is}) - \sigma(P_{io})] + (\overline{P_{io}} + \overline{P_{is}})^2 \quad (3)$$

and the dispersive as:

$$MSE_{disp} = 2(1 - CI)\, \sigma(P_{io})\, \sigma(P_{is}) \quad (4)$$

where $\sigma(x)$ is the SD of the x-variable, and CI is the previously mentioned spatial CI.

Furthermore, we also performed a Mann-Whitney U-test for checking OLAM and reanalysis accumulated precipitation data, for all selected events. This non-parametric test checks the null hypothesis that both data present the same distribution. For this, we adopted a p-value threshold of 0.05.

Special coding programs in the Python language were developed to perform the statistical analysis presented here. These programs are freely available at https://github.com/daniloceano/OLAM_validation.

3. RESULTS

This section presents the results of the determination of the main extreme weather events in the study region and the results of the OLAM numerical simulations. A brief description of the atmospheric conditions related to each event occurrence can be found in Text S1 in the Supplement.

3.1. Extreme events selection

The extreme events date of occurrence, associated impacts and atmospheric dynamics are presented in Table 1. We selected the major 12 extreme events for the recent past (i.e. 2000–2018). Most of the selected cases were extreme events that damaged urban areas and led to economic losses for the affected cities. The remaining events were associated with extreme wind speeds, storm surges and high waves that impacted the coastal infrastructure. Some of the selected events were already mentioned in the literature, such as the occurrence of events with high waves (E04, E06, E09, E10 and E11), strong winds (E04, E08 and E12) and heavy rainfall (E07 and E08). Four events (E01, E02, E03 and E05) had not already been mentioned by the scientific literature, and all of them were related to excessive precipitation. Therefore, our analysis resulted in the selection of events with a combination of hazards.

Event occurrence showed no clear seasonal pattern. The 2 most frequent event types, heavy rain (HR) and high wind speeds (HW), occurred preferably during warmer and colder months of the year, respectively. In general, during the austral winter, cold fronts pass through the region, while during the summer months, strong local convection in association with synoptic-scale phenomena (frontal systems, South American Low-Level Jet and South American Convergence Zone) enhances the strength of local thunderstorms.

All the selected events occurred in association with cyclonic or anticyclonic activity near the coastal area of SBr. Half of the events were related to cyclonic activity (one of them being a hurricane), nearly half were related to both cyclonic and anticyclonic transitory activity and a single event was related only to a stationary anticyclone. It was already expected that a high number of cyclogenetic events were related to

Table 1. Extreme events selected for numerical experiments and indicating start, end and peak (approximated) date. Peak hours are given in UTC. HR: heavy/persistent rainfall; SWd: strong winds; SS: storm surges; HW: high waves; CT: extreme cold temperatures. The atmospheric dynamic (AD) associated with the events were either anticyclonic (AC) or cyclonic (CS) activity or both. Scientific literature supporting the classification of an event as extreme is indicated, when available

Event	Year	Start	End	Peak	Impact	AD	Reference for classification
1	2018	10 Jan	16 Jan	11 Jan 18Z	HR	AC, CS	
2	2017	01 Jun	07 Jun	04 Jun 21Z	HR	AC, CS	
3	2011	06 Sep	09 Sep	08 Sep 09Z	HR	CS	
4	2011	25 May	30 May	28 May 06Z	SWd, HW, SS	CS	Candella & Souza (2013)
5	2011	18 Jan	23 Jan	21 Jan 21Z	HR	AC, CS	
6	2010	09 Apr	11 Apr	10 Apr 09Z	SWd, HW, SS	AC, CS	da Silva (2013)
7	2008	18 Nov	25 Nov	22 Nov 12Z	HR	AC	Fraga (2009), Minuzzi & Rodrigues (2008), Dos Santos et al. (2014)
8	2008	02 May	04 May	03 May 21Z	HR, SWd, HW	AC, CS	Guimarães et al. (2014), Sausen et al. (2009)
9	2007	28 Jul	30 Jul	28 Jul 12Z	HW	CS	Guimarães et al. (2014)
10	2006	01 Sep	06 Sep	03 Sep 18Z	HW, CT	CS	Guimarães et al. (2014), Parise et al. (2009)
11	2005	08 Aug	13 Aug	10 Aug 09Z	SWd, HW	AC, CS	Melo Filho et al. (2006)
12	2004	18 Mar	28 Mar	28 Mar 06Z	HR, SWd, SS	CS	Dias Pinto & Da Rocha (2011), Pezza & Simmonds (2005)

impacts such as erosion and coastal flooding. However, the impacts of anticyclonic systems are often not analyzed by the literature, although the orographic rain caused by the easterly flow from the anticyclone together with the mountains close to the coast in this region results in flash floods events (Rodrigues & Ynoue 2016).

3.2. Model results evaluation

Fig. 2 shows the total accumulated precipitation comparison between the model results and observations (TRMM and GPM) for each case study. The results show that for most of the events except E07 and E12, OLAM underestimated the maximum values of accumulated precipitation. However, except for E01, E02 and E06, the visual subjective analysis indicated that the spatial distribution was well represented, including the regions where maximum precipitation occurred.

The results from the statistical analysis of total accumulated precipitation are presented in Table 2. It can be seen both from the difference between OLAM and the reanalysis and from the bias that OLAM underestimated total precipitation for most events, except for E07 (bias: 0.64). The largest model bias was found for E02, E03 and E05. For those events, the largest part of the error was explained by the MSE_{diss}, which indicates that the bias associated with those events was mainly caused by an underestimation of precipitation intensity, although only E02 presented a CI value lower than 0.7. For E07, E08, E11 and E12, the opposite was true, as the associated MSE_{diss} was larger than the MSE_{disp}. Meanwhile, for the remaining events (E04, E06, E09 and E10), the difference between both MSE components was no greater than 5 mm, which indicates that for those events, both amplitude and phase errors contributed equally to the model bias.

Statistical spatial correlation between the observed and simulated accumulated total precipitation presented heterogeneous results. The lowest spatial correlations were found for E08, E01, E02 and E06 (0.47, 0.49, 0.53, 0.58, respectively). For the remaining events, the model presented correlation values ranging from 0.60 to 0.83 Additionally, we performed the Mann-Whitney *U*-test for all events. For all of them, the null hypothesis was rejected, i.e. the model and the reanalysis data presented different distributions.

To evaluate overall domain accumulated precipitation, we performed a comparison between the model and the TRMM/GPM spatial distributions (Fig. 3). This comparison indicates that the model simulated well the precipitation behavior for most events, as both modeled and estimated precipitation distributions presented similar slopes. However for most events except E07, E08 and E12, the GPM/TRMM presented higher frequency for higher precipitation points. Nevertheless, this analysis confirms that the model underestimates precipitation for most of the selected events. For E07 and E12, the 2 most important events, OLAM simulated higher maximum precipitation values than the TRMM estimates. However,

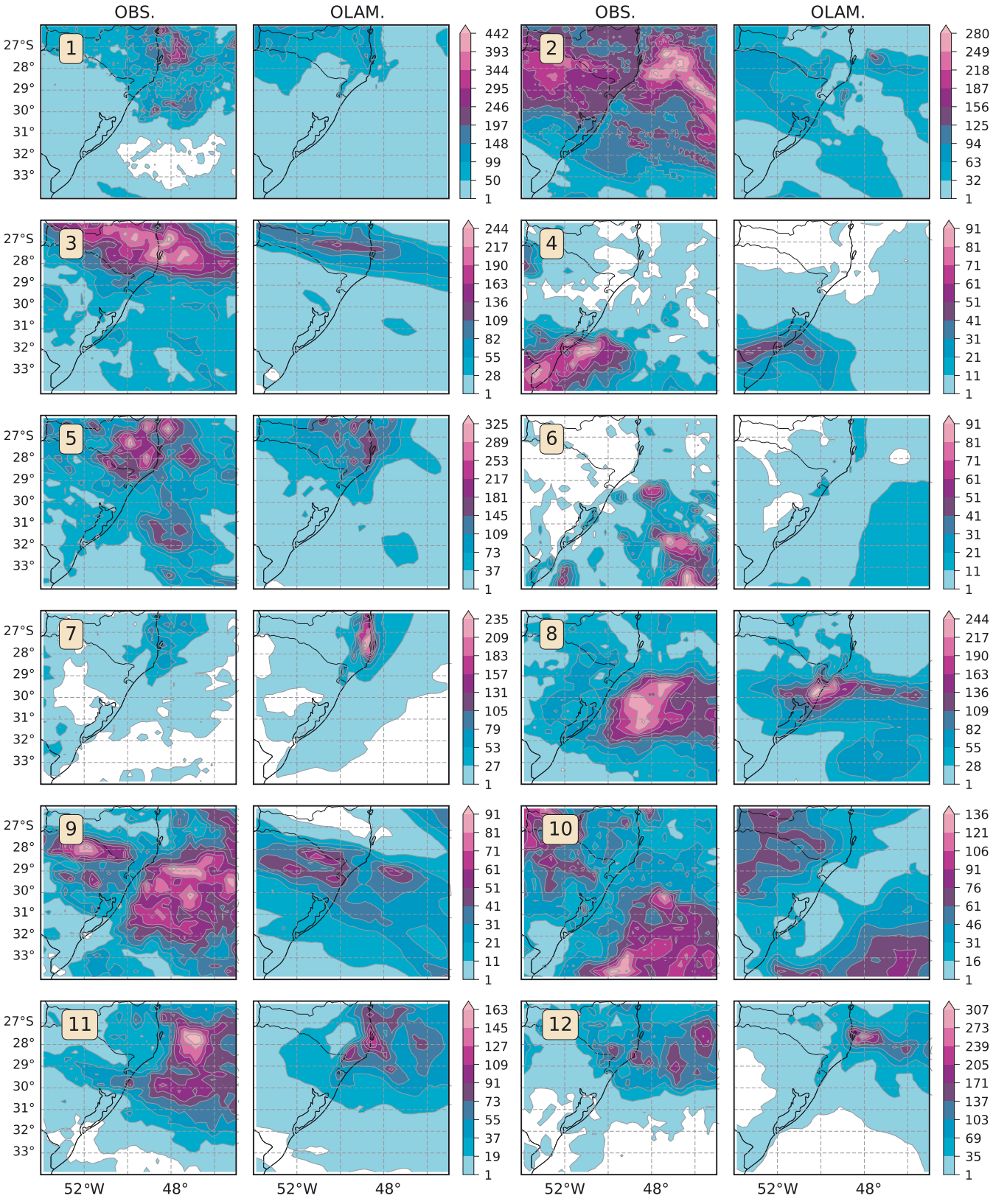

Fig. 2. Ocean–Land Atmosphere Model (OLAM) and Global Precipitation Measurement (GPM) mission or Tropical Rainfall Measuring Mission (TRMM) accumulated precipitation (OBS) for each selected extreme event (numbered 1–12). Due to availability of data, GPM fields were used for events 1 and 2 and the TRMM for the remaining events. Color intervals in mm

Table 2. Error and statistics indices calculated for Ocean–Land Atmosphere Model (OLAM) and reanalysis (Global Precipitation Measurement mission or Tropical Rainfall Measuring Mission) total accumulated precipitation (TAP), for all selected events: TAP (sum over the whole domain) for reanalysis (R) and OLAM (O) data and respective SDs, model bias, RMSE, square root of the dissipative and dispersive components of the mean square error (MSE_{diss} and MSE_{disp}, respectively) and spatial correlation index (CI)

Event	R_TAP (10^5 mm)	SD (mm)	O_TAP (10^5 mm)	SD (mm)	Bias (mm)	RMSE (mm)	$(MSE_{diss})^{1/2}$ (mm)	$(MSE_{disp})^{1/2}$ (mm)	CI
1	3.598	56.63	2.131	31.88	−20.38	53.67	43.04	32.06	0.49
2	8.780	60.20	2.678	19.05	−84.75	99.76	32.80	94.22	0.53
3	0.802	55.86	0.307	28.14	−41.82	55.35	23.34	50.17	0.83
4	0.168	20.22	0.096	10.53	−6.09	14.94	9.58	11.45	0.78
5	0.930	54.69	0.451	37.68	−40.43	56.29	35.24	43.87	0.70
6	0.132	17.32	0.084	5.33	−4.01	15.39	8.78	12.64	0.58
7	0.114	16.28	0.121	27.04	0.64	19.98	16.82	10.77	0.68
8	0.755	52.53	0.524	35.71	−19.50	51.34	44.40	25.75	0.47
9	0.388	21.92	0.226	13.52	−13.64	22.26	15.44	16.02	0.60
10	0.597	28.08	0.413	21.92	−15.49	26.62	20.73	16.67	0.65
11	0.413	34.45	0.278	24.41	−11.42	28.42	23.99	15.20	0.66
12	0.462	47.96	0.274	35.72	−15.92	37.98	32.21	20.08	0.70

for those cases, TRMM may have underestimated precipitation. Overall, the results indicate that the setup chosen for the experiments presented promising results for simulations of extreme precipitation events in this particular coastal study area, despite the underestimation found in most of the events.

Fig. 4 shows the daily evolution of accumulated precipitation, so the correspondence between event evolution in the model and in the reanalysis can be assessed. The model underestimated overall daily accumulated values for most events except for E07, E12 (as shown for the total accumulated) and E06. In the case of E06, although the values of daily precipitation were higher for OLAM, it underestimated the maximum values and presented the precipitation more spread over the domain, when compared to the reanalysis (Figs. 2 & 3).

Except for E03 and E12, the model was able to indicate correctly the days in which precipitation occurred and the tendency, i.e. if the precipitation amount was increasing or decreasing. For E03, the model was not able to represent well the initial tendency and precipitation amount, but as indicated by Fig. 2 and the MSE values, it was able to indicate the spatial distribution of it, which is reflected in the spatial CI values. Meanwhile, in the E12 case, the model overestimates precipitation on the first 4 d of simulation and on Days 9 and 11, but it underestimates precipitation on the last days of the simulation. For the remaining events, the precipitation tendency is well represented, except for the underestimations presented in the OLAM simulations.

The temporal correspondence of the model and estimated daily accumulated precipitation can also be assessed through Fig. 4. For most events, there is an initial low correlation score between the model and the reanalysis which generally increases during the simulation period and, for some events, drops during moments when the daily accumulation differs from both data. For example, the initial spike (from 0 to 0.7, approximately) in the correlation values in E08 is related to the model being able to represent accumulated precipitation in the first days of the simulation. However, the disagreement between estimated and simulated precipitation maxima on Days 4 and 5 leads to a drop in correlation values (from 0.6 to 0.4, approximately). A distinct behavior is noted for E12, in which the model was not capable of correctly representing the time periods of precipitation, but the final accumulated precipitation resulted in a CI of approximately 0.6, as the final values of total accumulated precipitation were similar.

In Fig. 5, we compared the simulated wind field and sea level pressure (SLP), during each event peak time, with the estimates from MERRA-2. Although OLAM had consistently underestimated the intensity of low-pressure zones, overall there was good agreement between simulations and observations for both wind and SLP data. This underestimation bias was evident especially for E02 and E11, corresponding to cold front winter systems. Nevertheless, for E04, the OLAM SLP and wind results were consistent with the ECMWF model data studied by Candella & Souza (2013). Also, the simulated cyclone position for E08 and E12 matched the synoptic charts analyzed by Sausen et al. (2009) and the tracking calculated by Pezza & Simmonds (2005), respectively. The model presented consistent results for the high-pressure

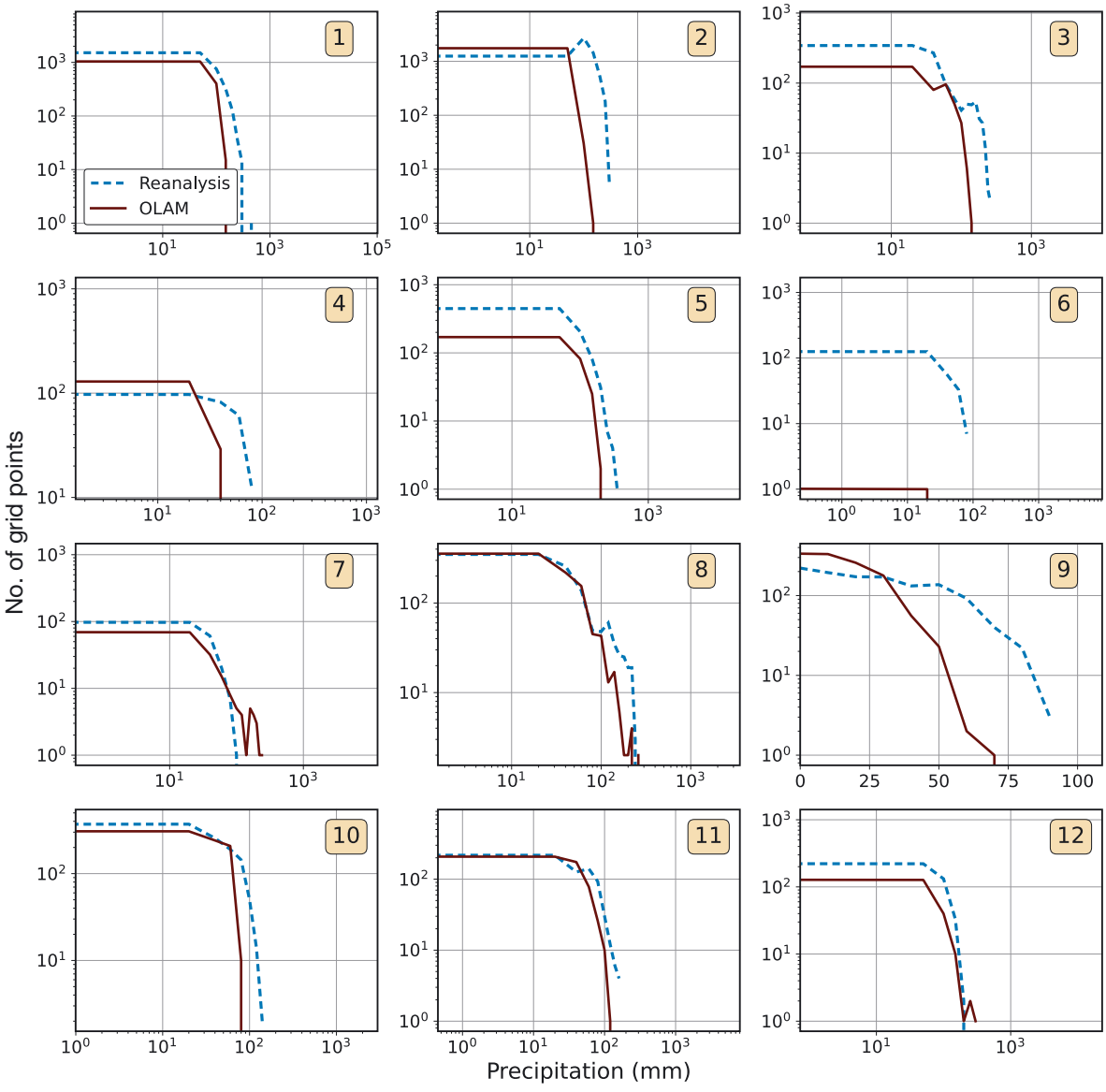

Fig. 3. Precipitation distribution integrated for the whole domain for the 12 selected extreme events (numbered 1–12). The *x*-axes represent the amount of precipitation, while the *y*-axes are the frequency of each class (represented by the number of grid points). Data corresponded to total accumulated precipitation during all simulation times, which was 10 d except for events 7 (11 d) and 12 (18 d)

zones, for both intensity and location, and overall there was a much higher spatial correlation as compared to the precipitation fields.

For E04 and E07, the model was able to represent the correct intensity of the minimum low pressure for each event peak time, while for E01, E05, E06, E09, E10 and E12, it was overestimated by 1 to 2 hPa (Table 3). This allowed a good representation of wind speed and direction along the SBr coast and adjacent areas (Fig. 5). For the remaining events (E02, E03, E11 and E12), the misrepresentation of either the intensity or the position of the minimum pressure zones resulted in erroneous wind speed and direction along the SBr coast. Regarding the high-pressure zones, OLAM was able to overall correctly reproduce their amplitude, as for most events it was either equal or from 1 to 2 hPa lower than the observed field.

The model bias for each event peak time (Table 3) indicates that there was an overall overestimation of the SLP across the domain, although for most cases, it was of approximately 1 hPa or less. Meanwhile, all CIs were higher than 0.9, indicating a good simulation of the SLP fields by OLAM. Regarding the MSE, for E01, E02, E03, E05, E07, E08, E10, E11 and E12,

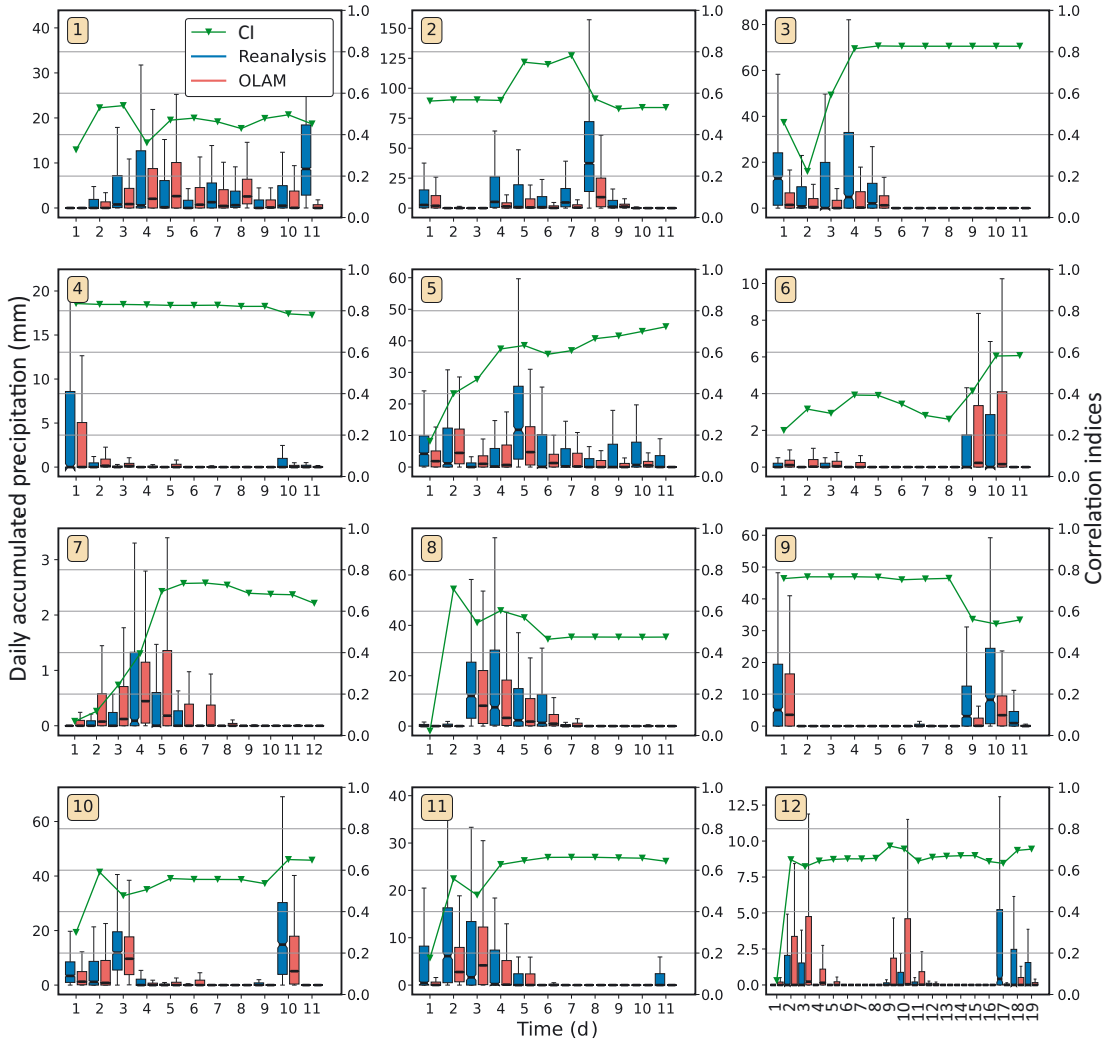

Fig. 4. Box plots of Ocean–Land Atmosphere Model (OLAM) and reanalysis (Global Precipitation Measurement [GPM] mission or Tropical Rainfall Measuring Mission [TRMM]) daily accumulated precipitation and respective correlation indices (CIs) for each day for the 12 selected extreme events (numbered 1–12). The box extends from the lower to upper quartile values of the data, the midline is the median and the whiskers represent the full range of data. CIs were calculated using the total accumulated along each event simulation instead of daily data

the dominant component of the error was the MSE_{diss}, while for E04, E06 and E09, the MSE_{disp} prevailed. Thus, for most events, the existing bias could be explained mainly by overestimation of the SLP fields, while for the remaining events, misplacement of the low- and/or high-pressure zones was the main reason for the observed bias.

There was also good agreement between the temporal evolution of the simulated and estimated SLP field, represented by the box plots in Fig. 6. The results show that the model is able to represent the evolution of the mean, maximum and upper quartile SLP values, while the minima and lower quartiles were often overestimated. For all events, during most days the correlation values remained higher than 0.8, and eventual decreases were often related to deepening of mean SLP, probably associated with the passage or intensification of low-pressure systems in the domain. This is especially evident for E01, E02, E03, E04, E08, E10 and E11. For E01, E02 and E04, the drops in correlation values are related to model overestimation of precipitation on Days 9 and 11 (E01), on Days 3 and 8 (E02) and from Day 7 to 10 (E04). For Day 6 of E03, although the correlation score decreased from approximately 1 to 0.7, there is no apparent overestimation of the SLP by the model, which indicates that the error might be related to the misplacement of pressure zones, which can also be observed to some extent in Fig. 3. A similar pattern can be observed on Day 8 of E08. For E05 and E06, there is little variation in the

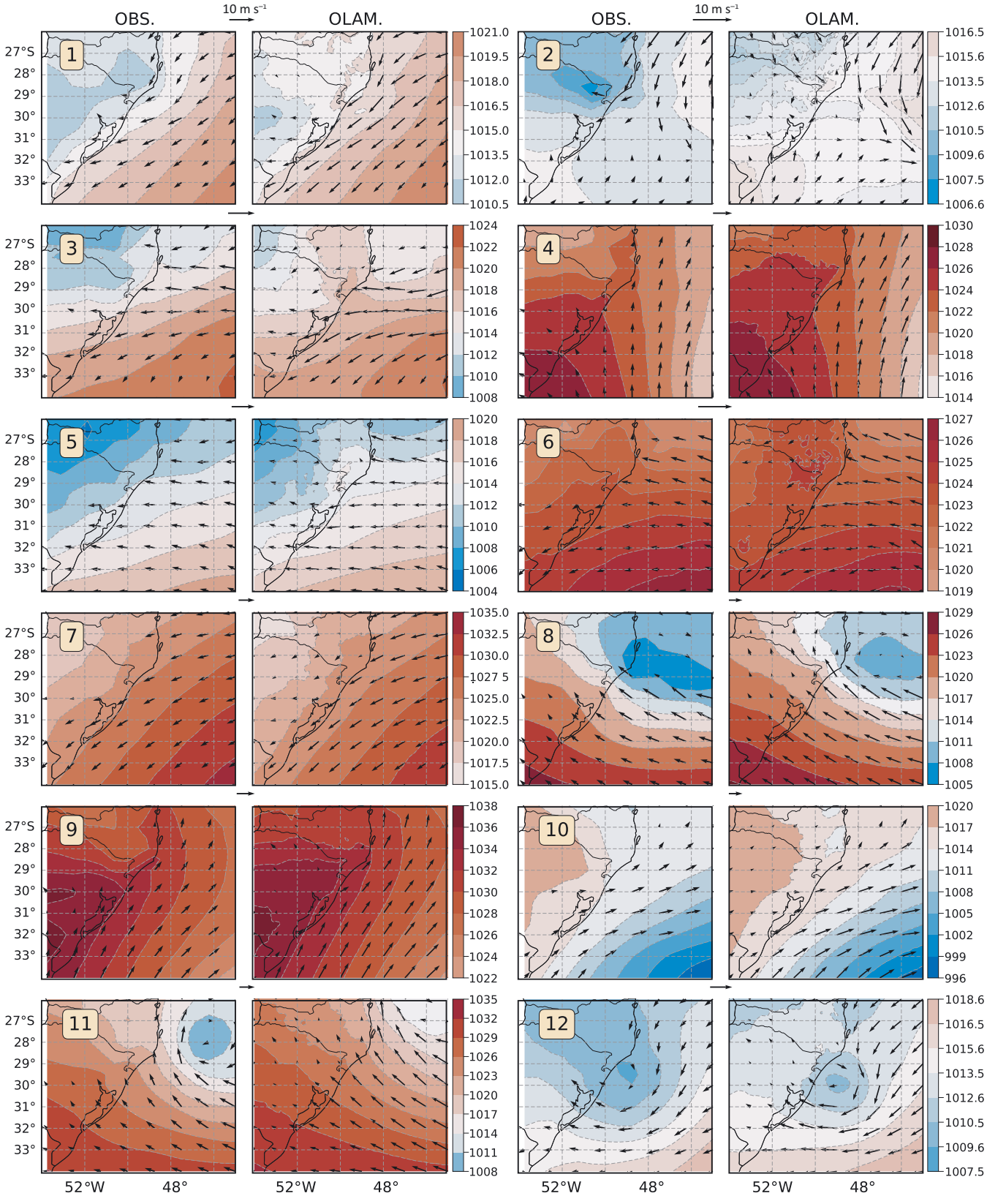

Fig. 5. Ocean–Land Atmosphere Model (OLAM) and Modern-Era Retrospective Analysis for Research and Applications, Version 2 (MERRA-2) sea level pressure (shaded, units in hPa) and winds (vectors) for peak time of the selected events (1–12). For OLAM and MERRA-2, (OBS) wind vector data are shown for only every 20 and 2 grid points, respectively, as using the original data points made visualization confusing

Table 3. Same as Table 2 but for sea level pressure values, presenting the reanalysis (R) and model (O) maximum (max) and minimum (min) values

Event	R_max (hPa)	R_min (hPa)	SD (hPa)	O_max (hPa)	O_min (hPa)	SD (hPa)	Bias (hPa)	RMSE (hPa)	$(MSE_{diss})^{1/2}$ (hPa)	$(MSE_{disp})^{1/2}$ (hPa)	CI
1	1020	1011	2.63	1021	1012	2.17	1.03	1.28	0.33	1.28	0.97
2	1015	1007	1.72	1015	1011	0.93	1.46	1.83	0.57	2.76	0.82
3	1022	1008	3.87	1022	1012	2.38	0.83	2.05	1.24	2.90	0.93
4	1028	1016	2.83	1028	1016	2.87	0.65	1.31	1.23	0.43	0.92
5	1019	1005	3.39	1018	1007	2.71	1.09	1.49	0.50	1.65	0.97
6	1027	1019	1.68	1026	1020	1.35	0.17	0.80	0.48	0.14	0.90
7	1034	1017	3.92	1032	1017	3.70	−0.94	1.04	0.04	0.93	1.00
8	1027	1006	6.01	1028	1010	5.27	1.48	1.86	0.46	2.75	0.99
9	1036	1023	3.07	1036	1024	2.89	0.50	1.20	1.08	0.29	0.94
10	1019	996	5.03	1019	997	4.88	0.99	1.16	0.14	1.01	1.00
11	1032	1009	6.20	1033	1014	4.97	2.44	2.97	1.11	7.49	0.98
12	1018	1009	2.15	1018	1010	1.64	1.30	1.51	0.31	1.95	0.96

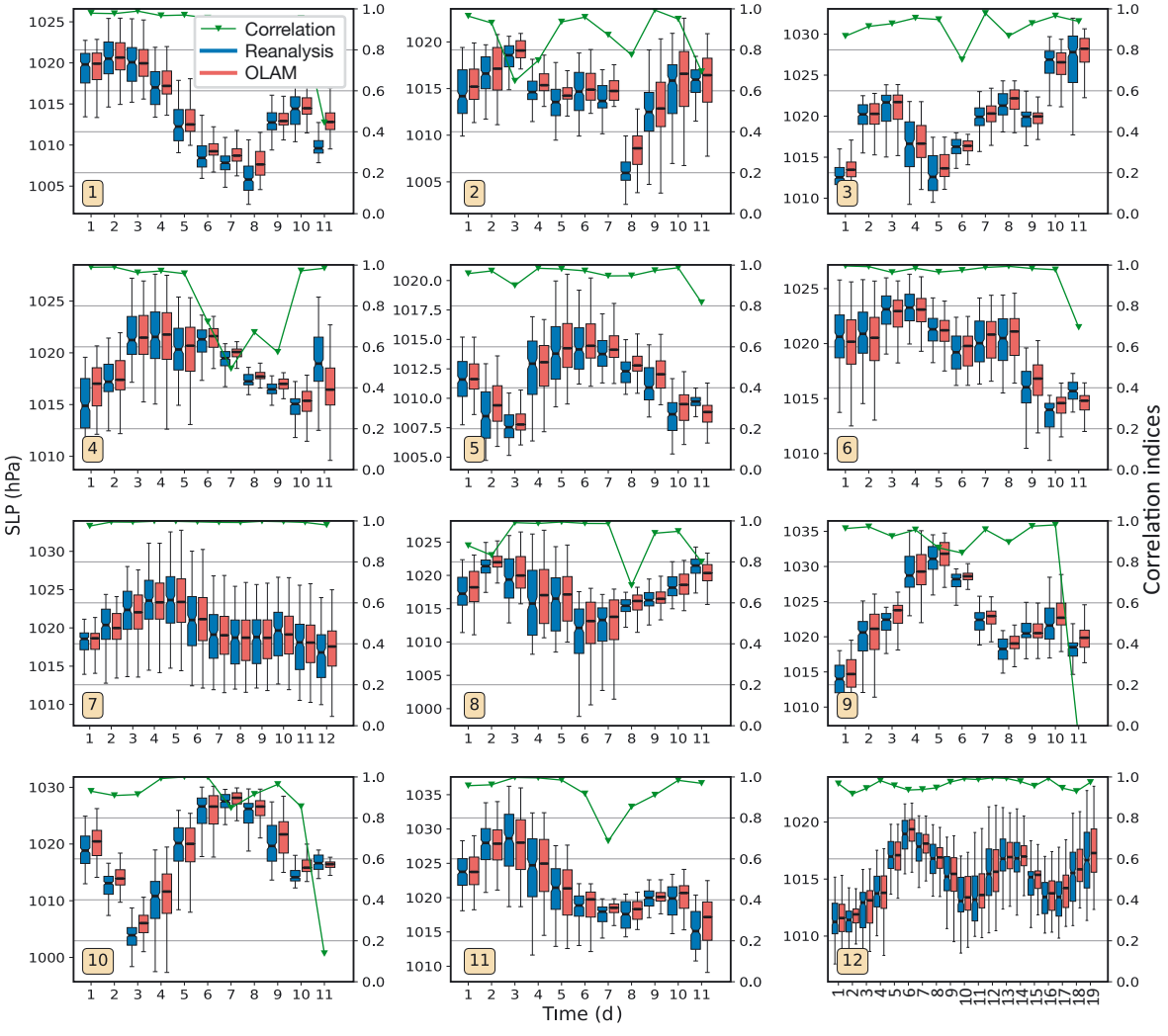

Fig. 6. Same as Fig. 4 but for daily mean sea level pressure (SLP)

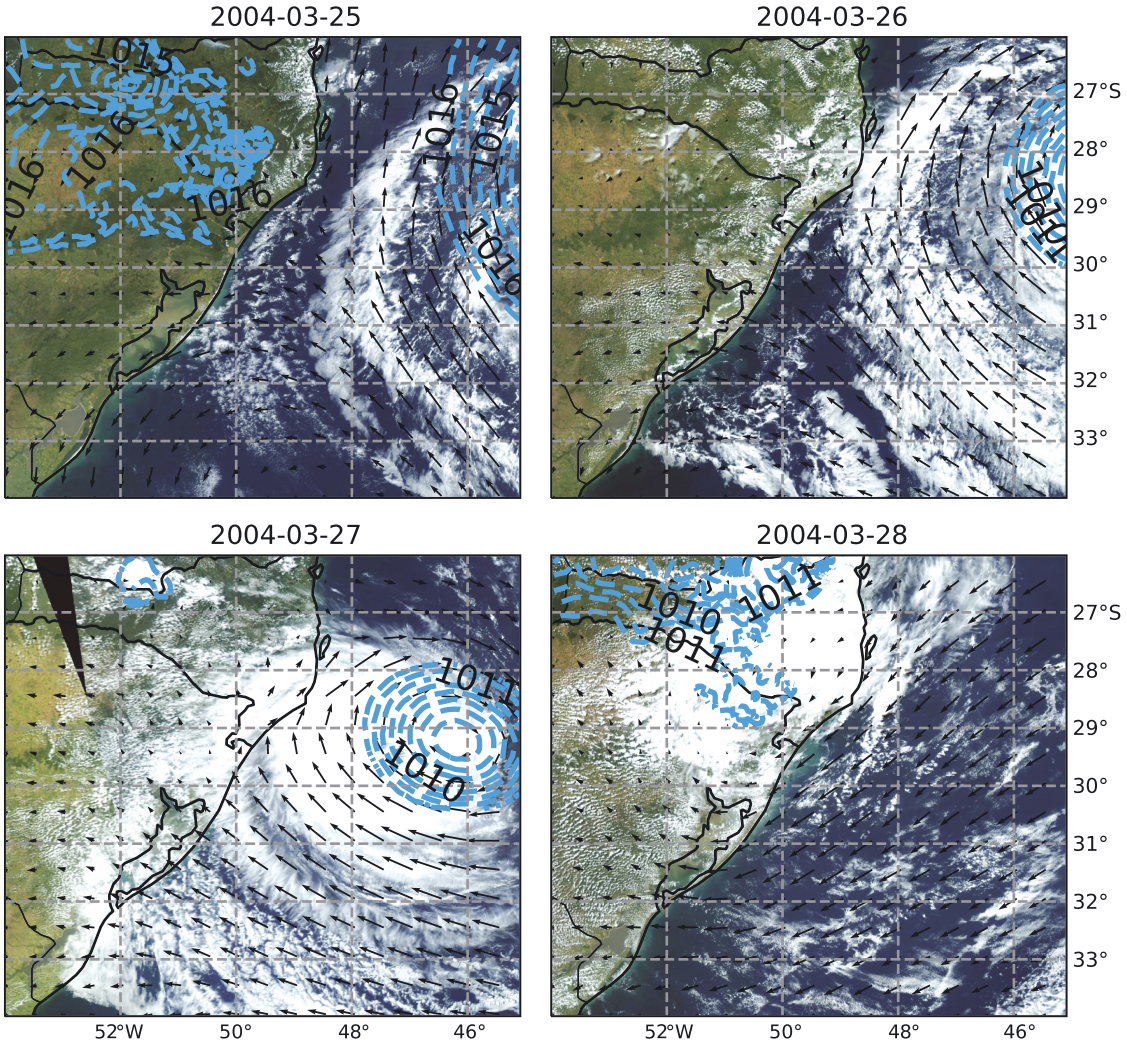

Fig. 7. Aqua/MODIS satellite image showing Hurricane Catarina (event 12) developments. Aqua/MODIS imagery shown is for 16:30 h UTC. Superimposed are the Ocean–Land Atmosphere Model surface wind vectors and minimum contours of sea level pressure for 15:00 h UTC of the same day

correlation apart from a decrease by the last day. E09 and E10 presented a similar pattern apart from some variation during the middle of the simulation, related to overestimations by OLAM. Meanwhile, for E07 and E12, the correlation was high during most of the simulation periods, as the model was able to accurately represent the SLP quartiles, maxima and minima. The positive bias for the minimum SLP may be responsible for lower precipitation in some cases.

Model performance for the wind field was directly correlated with its ability to represent high- and low-pressure systems. Thus, when low-pressure systems were offset, there was also a mismatch between the estimated and simulated wind intensity and direction near the system center. Nevertheless, the wind direction and intensity across the analysis domain closely matched those estimated by MERRA-2. To illustrate the model's ability to represent wind and SLP fields related to the extreme events presented here, we compared the OLAM results with the Aqua satellite image for the Hurricane Catarina event for the days before and after its landfall on the southern coast of the SC state (Fig. 7). The results show that there is a good correspondence between the modeled and the actual eye of the hurricane despite the time lag between the observation and model output.

To access model performance at the local level, we compared model results with precipitation and temperature data from all available INMET meteorological stations for the study area (Fig. 8). This analysis included only the event time period indicated in Table 1, which does not represent the entire simulation time. Temperature data were available for 00Z, 12Z and 18Z, while precipitation corresponded to

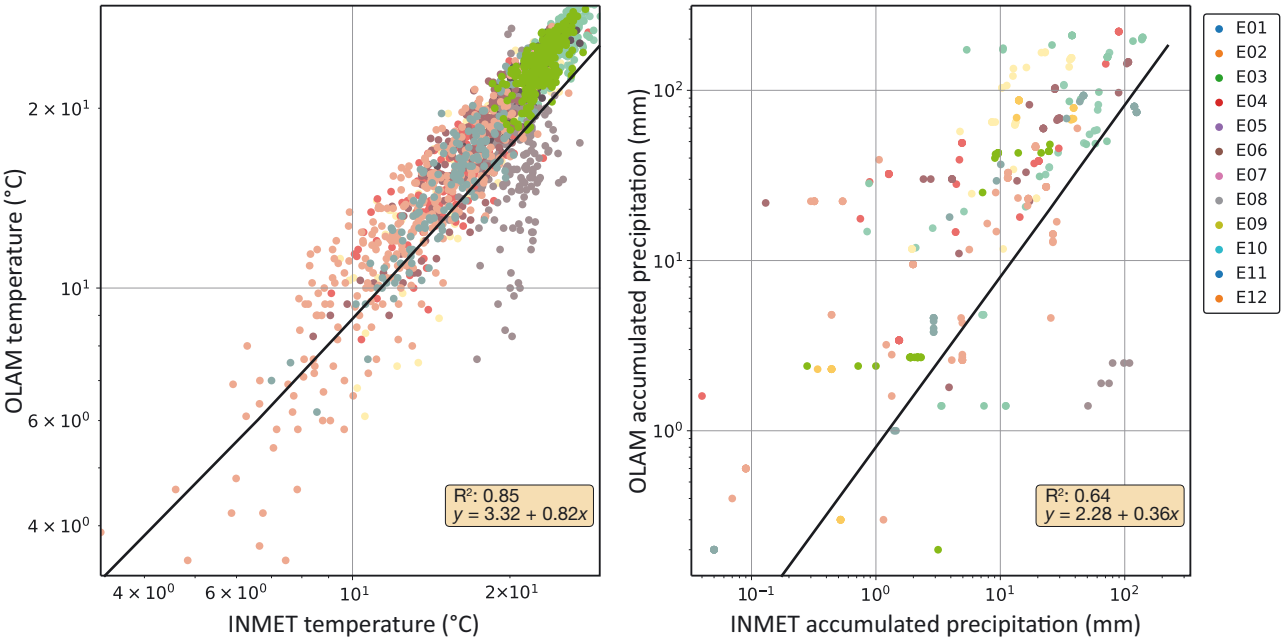

Fig. 8. Comparison between simulated and observed temperature (left) and accumulated precipitation (right, logarithm scale) for all 12 events (E01–E12) and Instituto Nacional de Meteorologia (INMET) weather station described in Section 2.4. Temperature data correspond to instantaneous values (at 00Z, 12Z and 18Z), and precipitation corresponds to daily accumulated values. OLAM: Ocean–Land Atmosphere Model

daily accumulated values. This analysis showed a good correspondence for temperature, which shows a good capacity of the model to simulate the local daily cycle. However, the analysis indicated a negative bias by modeled precipitation data but with better results for higher precipitation. This precipitation bias was not related to individual stations; instead, model accuracy changed according to each event. The same could be observed when comparing the accumulated precipitation spatial distribution between model results and GPM/TRMM data (Fig. 2). For both precipitation and temperature data, the E05 case was systematically underestimated by OLAM.

4. DISCUSSION

The mid-latitude region of the Southern Hemisphere is strongly influenced by Rossby planetary waves that travel around the region in approximately 4 to 6 d. On the other hand, the surface–atmosphere–ocean interface produces strong temperature gradients that affect surface fluxes like sensible and latent heat fluxes. Representing both the propagation of planetary waves and simultaneously the heterogeneity of the surface and its effects on local circulation is of fundamental importance for a good representation of mesoscale processes. In this study, the presented methodology allowed us to represent these phenomena of global and local scales simultaneously in the interface of the coastal region of southern Brazil using a state-of-the-art modeling approach.

A total of 12 extreme weather case studies were performed by OLAM, and results were compared with observations and reanalysis data. Although the model presented a systematic bias of underestimating precipitation, the accuracy varied among the selected events, which might be related to distinct causes. E01 and E02 were among the events with lower CIs and larger biases (Table 2). For those cases, the atmospheric conditions related to the development of the extreme precipitation include the presence of the South American Low-Level Jet, a phenomenon dependent on remote features, such as convection in the Amazon basin and interactions with the complex topography of the Andes (Wang & Fu 2004, Insel et al. 2010). However, in the model setup chosen for the current experiments, there is low resolution in the Andes region, which might affect the model's capability to represent the low-level jet and, thus, to represent the convective systems associated with this phenomenon. E05, which also presented one of the highest negative biases and lowest correspondences with the INMET station data (Fig. 8), was also related to low-level jet moisture transport from the Amazon region. Therefore, despite computational constraints, future

studies investigating the effects of better resolving the Andes mountain region on the simulation of extreme precipitation events for SBr, related to moisture transport from the Amazon region, are indicated.

Promising results were achieved for the 2 most important events for this coastal area, the Itajaí Valley flooding in 2008 (E07) and Hurricane Catarina (E12). For both events, the CI was approximately 0.7, whereas for the former, the model presented a positive bias of 0.64 mm. For E07, the orographic effects are important for representing shallow convection in the SC state region, where mountain ranges are close to the coastal plain (Rodrigues & Ynoue 2016). This highlights the importance of adopting high resolution for regions with complex and heterogeneous topography such as the coastal region of SBr.

Meanwhile, the Hurricane Catarina tropical transition was associated with environmental changes in atmosphere energy fluxes and also sea–air interactions (Veiga et al. 2008, Vianna et al. 2010). So, even though precipitation related to the event presented a negative bias and phase errors associated with daily accumulated values (Fig. 4), the accurate representation of the system position and temporal evolution (Fig. 7) indicates the model's capability to represent the heat fluxes and atmospheric dynamics related to this extreme event. For instance, simulations of this event with regional models demonstrated its sensitivity to air and sea temperature (Radu et al. 2014), so improvements on the model's cold bias (Fig. 8) or prescription of daily updated SSTs might result in better representation of such phenomena.

When comparing the OLAM data with the reanalysis, the SLP fields presented better results than did the accumulated precipitation. For the SLP data, most CI values for the event peak time were higher than 0.9, except for E02 (0.82). For this event, it can be seen that the minimum pressure amplitude and spatial distribution for this snapshot diverged from the reanalysis (Fig. 5). This might be related to the model not accurately representing the low-level jet event and, thus, resulting in the observed negative precipitation bias, although further investigation on this matter is required. Overall, the good representation of the pressure zones, indicated by the correlation values, resulted in a good representation of wind speed and direction along the SBr coastal region. Also, despite some positive bias by the model (with a maximum value of 2 hPa), the temporal evolution of the pressure zones were overall well represented, as shown by the quartiles and correlation values in Fig. 6. The observed oscillation in the correlation values was often related to intensification of high- and/or low-pressure zones that were not completely represented by the model.

The results show that although temperature and surface atmospheric pressure were overall well represented, the precipitation amount forecast is still underpredicted for this coastal region. However, the positive bias for surface pressure and negative bias for land surface fluxes may be partially responsible for the overall rainfall misrepresentation. The results point out, therefore, that improving these modeling variables may improve future forecasting of these coastal extreme events, and these should be carried out in future numerical studies.

Figs. 9 & 10 present a snapshot of sensible and latent heat flux emission for each of the 12 cases studied. These fluxes represent surface interaction with the atmosphere. The sensible heat flux responds to surface temperature, radiation and vertical air velocity near the boundary layer (Fig. 7). Also, the latent heat flux shows the evaporation of surface water in addition to the transpiration of local vegetation (Fig. 8). Soil moisture, radiation and temperature conditions are critical in controlling the evaporation and transpiration of vegetation that is controlled by stomatal resistance (Walko et al. 2000). The generation of these surface fluxes produces local breeze circulations such as the sea breeze and mountain breeze that are of great importance for the establishment of moisture flow and the local water cycle.

For comparison, the OLAM sensible heat flux (mean ± SD) for the snapshots presented in Fig. 9 was 52 ± 32 W m^{-2}, compared to 82 ± 43 W m^{-2} from the MERRA-2 reanalysis. For the latent heat flux, the OLAM results were 159 ± 58 W m^{-2}, compared to 212 ± 68 W m^{-2} from MERRA-2. This provides clues about the source of bias in the model simulations. However, the corresponding Bowen ratio (sensible flux/latent flux) from OLAM and MERRA-2 are 0.32 and 0.39, respectively. Thus, we can consider a reasonable energy flux partition from the model results at this coastal region.

Phenomena such as heavy rainfall and rising sea levels can occur simultaneously and have impacts on densely populated coastal regions. Identifying the strengths and biases in modeling and improving the predictability of these extreme events have therefore become of great importance, as climate projections suggest an increase in the frequency and intensity of these events (IPCC 2013).

The ongoing Regional Oceanic and Atmospheric Downscaling-Brazilian Earth System Model (ROAD-BESM) project aims to downscale climate change projections from BESM and provide high-resolution

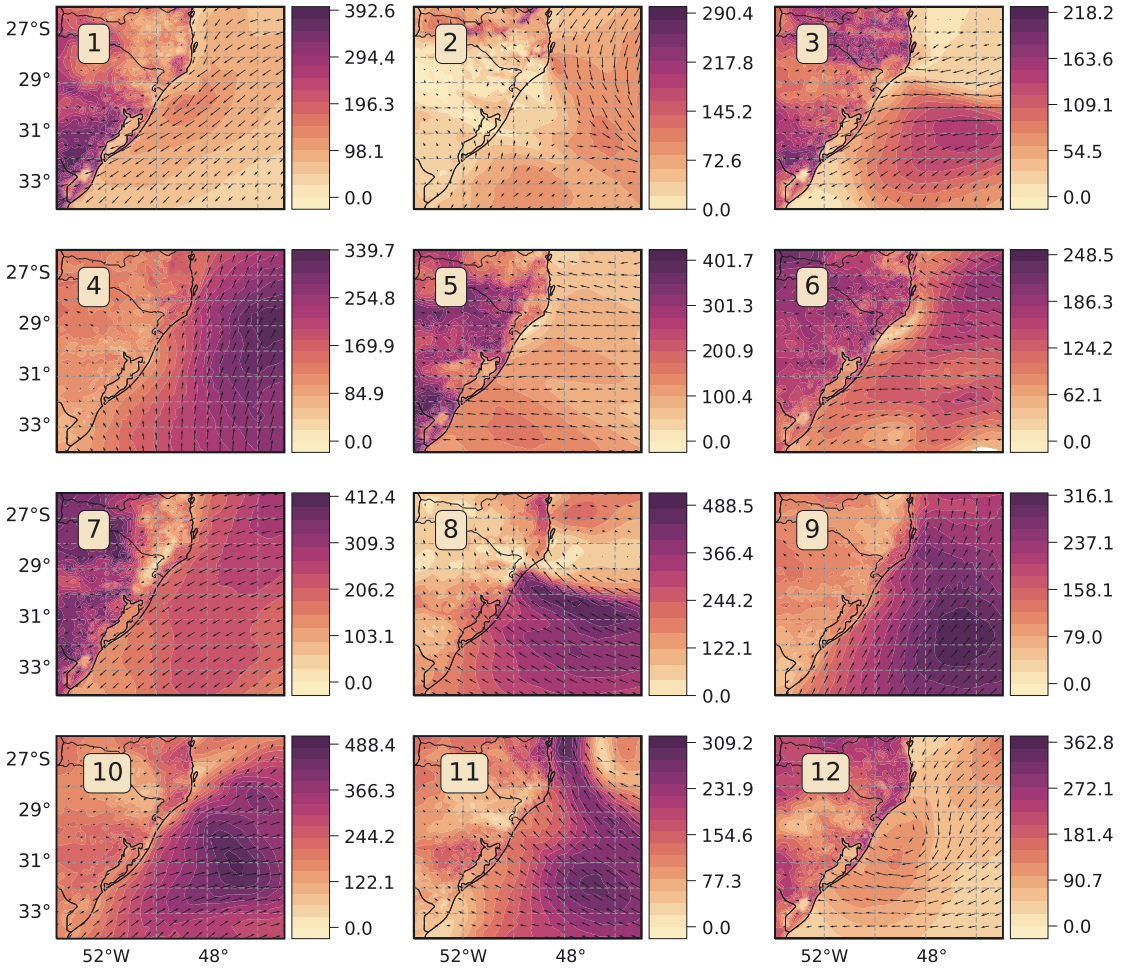

Fig. 9. Upward latent heat flux (W m^{-2}) and near-surface wind vectors simulated by the Ocean–Land Atmosphere Model for each event (1–12). For each case, we selected the time frame corresponding to the same day as the peak time, but the chosen hour was 15:00 h UTC

climate data for the coastal region of southern Brazil including future extreme event trends and coastline evolution. The atmospheric results of the present study will be applied as forcing fields for ocean models that allow simulating the variability of ocean currents and the dynamics of local waves. In this way, a more complete system might allow a better capacity to represent atmospheric and ocean conditions and therefore better predict the cases in which we have the simultaneous conditions of heavy rainfall and sea level rise. Nevertheless, the methodology presented for this coastal region can be adapted to any other regions. To do this, one may simply adapt the OLAM grid system to the center of the region of interest.

After evaluating the occurrence of extreme events in the southern coastal region of Brazil, we detected 12 cases. The simulation of these cases by OLAM allowed a good representation of temperature, surface pressure and rainfall distribution evolution. Although the results showed a bias for rainfall, the best results occurred for the most extreme cases showing the simulation capacity for these events. The method applied to this coastal region of southern Brazil allowed a detailed representation of the sensible and latent heat fluxes that are fundamental in the establishment of local mesoscale circulations. Therefore, these results show that this methodology is an important tool for coastal studies in any region of interest.

The model results including the bias and errors in this proposed setup show that several improvements may be carried out in the future. For instance, establishing a mesonet weather station network would help to improve the model's initial conditions and also provide data for the modeling evaluation. Also, an improved data assimilation system including remote sensing data would improve the model's initial condition. Furthermore, the spatial resolution adopted here of 6 km still is not a cloud-resolving

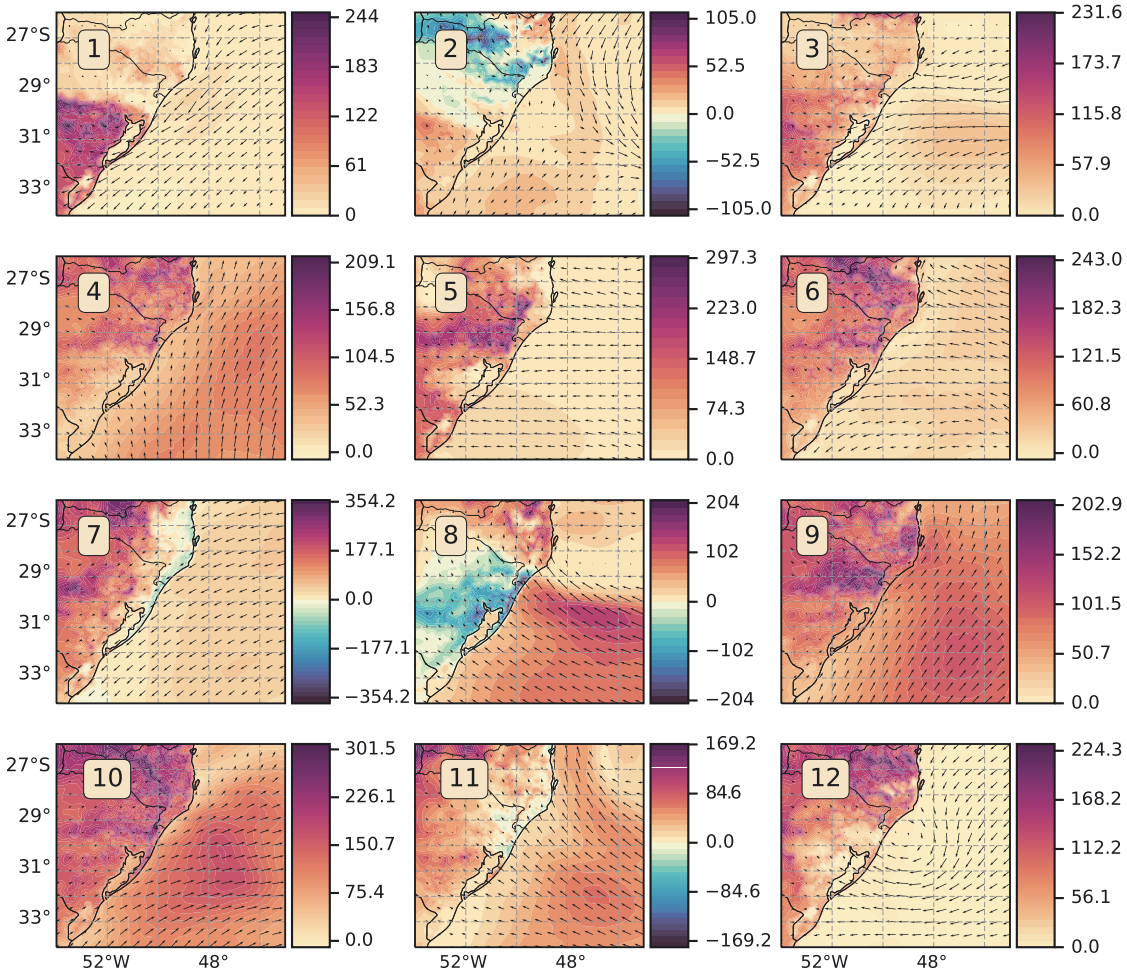

Fig. 10. Same as Fig. 9 but for sensible heat flux (W m^{-2})

model, and the cumulus parameterizations do not work properly in this spacing scale (see also Bryan et al. 2003, Hong & Dudhia 2012, Grell & Freitas 2014). Therefore, an improved model resolution on the order of 1 km should be carried out in the future. In addition, recent results show the importance of biomass-burning aerosols on cloud and rainfall formation in this region (Freire et al. 2020). Thus, further simulations on physical cloud microphysics should be carried out to better predict the correct precipitation, as it is a very important atmospheric variable responsible for the most catastrophic extreme events in this coastal region.

Acknowledgements. This study was financed in part by the Coordenação de Aperfeiçoamento de Pessoal de Nível Superior-Brasil (CAPES) through the project ROAD-BESM (88881146046201701). The research was conducted at the Federal University of Santa Catarina (UFSC). We thank 3 anonymous reviewers for their contributions and especially Pedro Leite da Silva Dias, Felipe Mendonça Pimenta and Paula Gomes da Silva for their insightful comments. The OLAM data that were used for the result analysis in this article as well as the OLAM namelist files can be found at the 4TU.Centre for Research Data (doi:10.4121/uuid:b5c1ef79-795e-42fc-b4b3-3487a0e6934e).

LITERATURE CITED

Albuquerque M da G, Leal Alves DC, Espinoza JM de A, Oliveira UR, Simões RS (2018) Determining shoreline response to meteo-oceanographic events using remote sensing and unmanned aerial vehicle (UAV): case study in southern Brazil. J Coast Res 85:766–770

Ambrizzi T, Reboita MS, da Rocha RP, Llopart M (2019) The state of the art and fundamental aspects of regional climate modeling in South America. Ann N Y Acad Sci 1436:98–120

Bryan GH, Wyngaard JC, Fritsch JM (2003) Resolution requirements for the simulation of deep moist convection. Mon Weather Rev 131:2394–2416

Buchard V, Randles CA, da Silva AM, Darmenov A and others (2017) The MERRA-2 aerosol reanalysis, 1980 onward.

Part II: evaluation and case studies. J Clim 30:6851–6872
Campos RM, De Camargo R, Harari J (2010) Caracterização de eventos extremos do nível do mar em Santos e sua correspondência com as reanálises do modelo do NCEP no sudoeste do Atlântico Sul. Rev Bras Meteorol 25:175–184
Candella RN, Souza SML (2013) Ondas oceânicas extremas na costa sul-sudeste Brasileira geradas por ciclone com trajetória anormal em maio de 2011. Rev Bras Meteorol 28:441–456
Carvalho LMV, Jones C, Liebmann B (2004) The South Atlantic Convergence Zone: intensity, form, persistence, and relationships with intraseasonal to interannual activity and extreme rainfall. J Clim 17:88–108
Chou SC, Lyra A, Mourão C, Dereczynski C and others (2014) Assessment of climate change over South America under RCP 4.5 and 8.5 downscaling scenarios. Am J Clim Change 03:512–527
Compagnucci RH, Salles MA (1997) Surface pressure patterns during the year over southern South America. Int J Climatol 17:635–653
da Silva PED (2013) Caracterização do padrão de ondas na costa do Brasil por meio de modelagem numérica. MSc thesis, Instituto Nacional de Pesquisas Espaciais, São José
Dias Pinto JR, Da Rocha RP (2011) The energy cycle and structural evolution of cyclones over southeastern South America in three case studies. J Geophys Res Atmos 116:1–17
Dos Santos CF, Tornquist CS, Marimon MPC (2014) Indústria das enchentes: impasses e desafios dos desastres socioambientais no vale do Itajaí. Geosul 29:197–216
Draper CS, Reichle RH, Koster RD (2018) Assessment of MERRA-2 land surface energy flux estimates. J Clim 31: 671–691
Easterling DR, Meehl GA, Parmesan C, Changnon SA, Karl TR, Mearns LO (2000) Climate extremes: observations, modeling, and impacts. Science 289:2068–2074
Ebisuzaki W, Zhang L (2011) Assessing the performance of the CFSR by an ensemble of analyses. Clim Dyn 37: 2541–2550
Farnham DJ, Doss-Gollin J, Lall U (2018) Regional extreme precipitation events: robust inference from credibly simulated GCM variables. Water Resour Res 54:3809–3824
Fernandes LG, Rodrigues RR (2018) Changes in the patterns of extreme rainfall events in southern Brazil. Int J Climatol 38:1337–1352
Fraga NC (2009) Enchentes urbanas no Vale do Itajaí, Brasil. 25 anos da enchente catástrofe de 1983 — reflexos socioambientais e culturais no século XXI. Encuentro Geógrafos da América Lat Caminando a una América Lat en Transformación 12, http://observatoriogeograficoamericalatina.org.mx/egal12/Procesosambientales/Impactoambiental/39.pdf
Freire JLM, Longo KM, Freitas SR, Coelho CAS and others (2020) To what extent biomass burning aerosols impact South America seasonal climate predictions? Geophys Res Lett 47:e2020GL088096
Frich P, Alexander LV, Della-Marta P, Gleason B, Haylock M, Klein Tank AMG, Peterson T (2002) Observed coherent changes in climatic extremes during the second half of the twentieth century. Clim Res 19:193–212
Garreaud RDD (2000) Cold air incursions over subtropical South America: mean structure and dynamics. Mon Weather Rev 128:2544–2559
Garreaud RDD, Vuille M, Compagnucci R, Marengo J (2009) Present-day South American climate. Palaeogeogr Palaeoclimatol Palaeoecol 281:180–195
Gebremichael M, Krajewski WF (2004) Assessment of the statistical characterization of small-scale rainfall variability from radar: analysis of TRMM ground validation datasets. J Appl Meteorol 43:1180–1199
Gelaro R, McCarty W, Suárez MJ, Todling R and others (2017) The Modern-Era Retrospective Analysis for Research and Applications, Version 2 (MERRA-2). J Clim 30:5419–5454
Gomes da Silva P, Dalinghaus C, González M, Gutiérrez O, Espejo A, Abascal AJ, Klein AHF (2016) Estimating flooding level through the Brazilian coast using reanalysis data. J Coast Res 75:1092–1096
Gordon AL (1989) Brazil-Malvinas confluence–1984. Deep-Sea Res A, Oceanogr Res Pap 36:359–384
Gramcianinov CB, Hodges KI, Camargo R (2019) The properties and genesis environments of South Atlantic cyclones. Clim Dyn 53:4115–4140
Grell GA, Freitas SR (2014) A scale and aerosol aware stochastic convective parameterization for weather and air quality modeling. Atmos Chem Phys 14:5233–5250
Guimarães PV, Farina L, Toldo EE (2014) Analysis of extreme wave events on the southern coast of Brazil. Nat Hazards Earth Syst Sci 14:3195–3205
Handmer J, Honda Y, Kundzewicz ZW, Arnell N and others (2012) Changes in impacts of climate extremes: human systems and ecosystems. In: Field CB, Barros V, Stocker TF, Qin D and others (eds) Managing the risks of extreme events and disasters to advance climate change adaptation: Special report of Working Groups I and II of the Intergovernmental Panel on Climate Change (IPCC). Cambridge University Press, Cambridge and New York, NY, p 231–290
Hermann ML de P (2014) Atlas de desastres naturais do estado de Santa Catarina: perìodo de 1980 a 2010. IHGSC, Florianopolis
Hong SY, Dudhia J (2012) Next-generation numerical weather prediction: bridging parameterization, explicit clouds, and large eddies. Bull Am Meteorol Soc 93: ES6–ES9
Hoskins BJ, Hodges KI (2005) A new perspective on Southern Hemisphere storm tracks. J Clim 18:4108–4129
Hou AY, Kakar RK, Neeck S, Azarbarzin AA and others (2014) The Global Precipitation Measurement mission. Bull Am Meteorol Soc 95:701–722
Huffman GJ, Bolvin DT, Nelkin EJ, Wolff DB and others (2007) The TRMM Multisatellite Precipitation Analysis (TMPA): quasi-global, multiyear, combined-sensor precipitation estimates at fine scales. J Hydrometeorol 8: 38–55
Insel N, Poulsen CJ, Ehlers TA (2010) Influence of the Andes Mountains on South American moisture transport, convection, and precipitation. Clim Dyn 35:1477–1492
IPCC (2013) Climate change 2013: the physical science basis. In: Stocker TF, Qin D, Plattner GK, Tignor MMB and others (eds) Contribution of Working Group I to the Fifth Assessment Report of the Intergovernmental Panel on Climate Change. Cambridge University Press, Cambridge
Karl TR, Easterling DR (1999) Climate extremes: selected review and future research directions. Clim Change 42: 309–325
Khanna J, Medvigy D, Fueglistaler S, Walko R (2017) Regional dry-season climate changes due to three decades of Amazonian deforestation. Nat Clim Chang 7:200–204
Kodama Y (1992) Large-scale common features of subtropical precipitation zones (the Baiu Frontal Zone, the SPCZ,

and the SACZ) Part I: characteristics of subtropical frontal zones. J Meteorol Soc Jpn 70:813–836

Krüger LF, da Rocha RP, Reboita MS, Ambrizzi T (2012) RegCM3 nested in HadAM3 scenarios A2 and B2: projected changes in extratropical cyclogenesis, temperature and precipitation over the South Atlantic Ocean. Clim Change 113:599–621

Kunkel KE, Pielke RA, Changnon SA (1999) Temporal fluctuations in weather and climate extremes that cause economic and human health impacts: a review. Bull Am Meteorol Soc 80:1077–1098

Liu Z (2016) Comparison of Integrated Multisatellite Retrievals for GPM (IMERG) and TRMM Multisatellite Precipitation Analysis (TMPA) monthly precipitation products: initial results. J Hydrometeorol 17:777–790

Machado AA, Calliari LJ, Melo E, Klein AHF (2010) Historical assessment of extreme coastal sea state conditions in southern Brazil and their relation to erosion episodes. Pan-Am J Aquat Sci 5:277–286

Marengo JA, Soares WR, Saulo C, Nicolini M (2004) Climatology of the low-level jet east of the Andes as derived from the NCEP–NCAR reanalyses: characteristics and temporal variability. J Clim 17:2261–2280

Marengo JA, Jones R, Alves LM, Valverde MC (2009) Future change of temperature and precipitation extremes in South America as derived from the PRECIS regional climate modeling system. Int J Climatol 29:2241–2255

Mechler R, Bouwer LM (2015) Understanding trends and projections of disaster losses and climate change: Is vulnerability the missing link? Clim Change 133:23–35

Medvigy D, Walko RL, Avissar R (2008) Modeling interannual variability of the Amazon hydroclimate. Geophys Res Lett 35:2–6

Medvigy D, Walko RL, Avissar R (2012) Simulated links between deforestation and extreme cold events in South America. J Clim 25:3851–3866

Medvigy D, Walko RL, Otte MJ, Avissar R (2013) Simulated changes in northwest US climate in response to Amazon deforestation. J Clim 26:9115–9136

Melo Filho E, Hammes GR, Franco D (2006) Estudo de caso: a ressaca de Agosto de 2005 em Santa Catarina. In: 2° Seminario e workshop em engenharia oceânica. FURG, Rio Grande, p 1–20

Mendes D, Souza EP, Marengo JA, Mendes MCD (2010) Climatology of extratropical cyclones over the South American–southern oceans sector. Theor Appl Climatol 100:239–250

Meyers MP, Walko RL, Harrington JY, Cotton WR (1997) New RAMS cloud microphysics parameterization. Part II: the two-moment scheme. Atmos Res 45:3–39

Minuzzi R, Rodrigues L (2008) Novembro com recordes de chuva em SC: 1000 mm em Blumenau. Setor de Previsão de Tempo e Clima, Epagri/Ciram

Mlawer EJ, Taubman SJ, Brown PD, Iacono MJ, Clough SA (1997) Radiative transfer for inhomogeneous atmospheres: RRTM, a validated correlated-k model for the longwave. J Geophys Res Atmos 102:16663–16682

Nunes AB, Da Silva GC (2013) Climatology of extreme rainfall events in eastern and northern Santa Catarina State, Brazil: present and future climate. Rev Bras Geofís 31: 413–425

Nuñez MN, Solman SA, Cabré MF (2009) Regional climate change experiments over southern South America. II: climate change scenarios in the late twenty-first century. Clim Dyn 32:1081–1095

Parise CK, Farina L (2012) Ocean wave modes in the South Atlantic by a short-scale simulation. Tellus A Dyn Meteorol Oceanogr 64:17362

Parise CK, Calliari LJ, Krusche N (2009) Extreme storm surges in the south of Brazil: atmospheric conditions and shore erosion. Braz J Oceanogr 57:175–188

Pezza AB, Simmonds I (2005) The first South Atlantic hurricane: unprecedented blocking, low shear and climate change. Geophys Res Lett 32:L15712

Pielke RA, Cotton WR, Walko RL, Tremback CJ and others (1992) A comprehensive meteorological modeling system — RAMS. Meteorol Atmos Phys 49:69–91

Radu R, Toumi R, Phau J (2014) Influence of atmospheric and sea surface temperature on the size of hurricane *Catarina*. QJR Meteorol Soc 140:1778–1784

Ramos da Silva R, Haas R (2016) Ocean global warming impacts on the South America climate. Front Earth Sci 4: 30

Ramos da Silva R, Gandú AW, Cohen JC, Kuhn P, Mota MA (2014a) Weather forecasting for eastern Amazon with OLAM model. Rev Bras Meteorol 29:11–22

Ramos da Silva R, Vitorino MI, Kuhn P, Ananias D dos S (2014b) Climate estimates for eastern Amazon with OLAM model. Rev Bras Meteorol 29:2–10

Randles CA, da Silva AM, Buchard V, Colarco PR and others (2017) The MERRA-2 aerosol reanalysis, 1980 onward. Part I: system description and data assimilation evaluation. J Clim 30:6823–6850

Reboita MS, Da Rocha RP, Ambrizzi T (2012) Dynamic and climatological features of cyclonic developments over southwestern South Atlantic Ocean. In: Veress B, Szigethy J (eds) Horizons in Earth science research, Vol 6. Nova Science Publishers, New York, NY, p 135–160

Reboita MS, da Rocha RP, de Souza MR, Llopart M (2018) Extratropical cyclones over the southwestern South Atlantic Ocean: HadGEM2-ES and RegCM4 projections. Int J Climatol 38:2866–2879

Reynolds RW, Smith TM (1994) Improved global sea surface temperature analyses using optimum interpolation. J Clim 7:929–948

Reynolds RW, Rayner NA, Smith TM, Stokes DC, Wang W (2002) An improved in situ and satellite SST analysis for climate. J Clim 15:1609–1625

Reynolds RW, Smith TM, Liu C, Chelton DB, Casey KS, Schlax MG (2007) Daily high-resolution-blended analyses for sea surface temperature. J Clim 20:5473–5496

Rodrigues MLG, Ynoue RY (2016) Mesoscale and synoptic environment in three orographically enhanced rain events on the coast of Santa Catarina (Brazil). Weather Forecast 31:1529–1546

Saha S, Moorthi S, Pan HL, Wu X and others (2010) The NCEP Climate Forecast System Reanalysis. Bull Am Meteorol Soc 91:1015–1058

Saha S, Moorthi S, Wu X, Wang J and others (2014) The NCEP Climate Forecast System Version 2. J Clim 27: 2185–2208

Salio P (2002) Chaco low-level jet events characterization during the austral summer season. J Geophys Res 107:4816

Salio P, Nicolini M, Zipser EJ (2007) Mesoscale convective systems over southeastern South America and their relationship with the South American low-level jet. Mon Weather Rev 135:1290–1309

Sausen TM, Ferreira CC, Antonio M, Hansen F, Saito SM (2009) Ciclone extratropical ocorrido em Maio de 2008 (SC e RS): gênese, evolução e avaliação das consequentes

inundações com o auxílio de geotecnologias. INPE, São José dos Campos

Seluchi ME, Marengo JA (2000) Tropical–midlatitude exchange of air masses during summer and winter in South America: climatic aspects and examples of intense events. Int J Climatol 20:1167–1190

Seluchi ME, Saulo AC, Nicolini M, Satyamurty P (2003) The northwestern Argentinean low: a study of two typical events. Mon Weather Rev 131:2361–2378

Sinclair MR (1995) A climatology of cyclogenesis for the Southern Hemisphere. Mon Weather Rev 123: 1601–1619

Smagorinsky J (1963) General circulation experiments with the primitive equations. Mon Weather Rev 91: 99–164

Stramma L (1989) The Brazil current transport south of 23° S. Deep-Sea Res A, Oceanogr Res Pap 36:639–646

Strohaecker TM (2004) Dinâmica populacional. In: Macrodiagnóstico da zona costeira e marinha do brasil. Ministério do Meio Ambiente, Brasília, p 59–74

Takacs LL (1985) A two-step scheme for the advection equation with minimized dissipation and dispersion errors. Mon Weather Rev 113:1050–1065

Taylor KE, Stouffer RJ, Meehl GA (2012) An overview of CMIP5 and the experiment design. Bull Am Meteorol Soc 93:485–498

Veiga JAP, Pezza AB, Simmonds I, Silva Dias PL (2008) An analysis of the environmental energetics associated with the transition of the first South Atlantic hurricane. Geophys Res Lett 35:1–6

Vianna ML, Menezes VV, Pezza AB, Simmonds I (2010) Interactions between Hurricane Catarina (2004) and warm core rings in the South Atlantic Ocean. J Geophys Res 115:C07002

Walko RL, Avissar R (2008a) The Ocean–Land–Atmosphere Model (OLAM). Part I: shallow-water tests. Mon Weather Rev 136:4033–4044

Walko RL, Avissar R (2008b) The Ocean–Land–Atmosphere Model (OLAM). Part II: formulation and tests of the nonhydrostatic dynamic core. Mon Weather Rev 136: 4045–4062

Walko RL, Avissar R (2011) A direct method for constructing refined regions in unstructured conforming triangular–hexagonal computational grids: application to OLAM. Mon Weather Rev 139:3923–3937

Walko RL, Cotton WR, Meyers MP, Harrington JY (1995) New RAMS cloud microphysics parameterization part I: the single-moment scheme. Atmos Res 38:29–62

Walko RL, Band LE, Baron J, Kittel TGF and others (2000) Coupled atmosphere–biophysics–hydrology models for environmental modeling. J Appl Meteorol 39:931–944

Wallemacq P, House R (2018) Economic losses, poverty and disasters 1998–2017. UNISDR and CRED, Brussels

Wang H, Fu R (2004) Influence of cross-Andes flow on the South American low-level jet. J Clim 17:1247–1262

Wang W, Xie P, Yoo SH, Xue Y, Kumar A, Wu X (2011) An assessment of the surface climate in the NCEP climate forecast system reanalysis. Clim Dyn 37:1601–1620

Wang Z, Zhong R, Lai C, Chen J (2017) Evaluation of the GPM IMERG satellite-based precipitation products and the hydrological utility. Atmos Res 196:151–163

World Bank (2016) Report of material damages and losses due to natural disasters in Brazil—1995–2014. Working Paper No. 111703. World Bank, Brasilia (in Portuguese)

Editorial responsibility: Oliver Frauenfeld, College Station, Texas, USA
Reviewed by: 3 anonymous referees

Submitted: May 22, 2020
Accepted: March 24, 2021
Proofs received from author(s): May 26, 2021